Space charges and defect concentration profiles at complex oxide interfaces

Felix Gunkel[*] and Rainer Waser

Institute for Electronic Materials, IWE2, RWTH Aachen University, Aachen, Germany
and Peter Gruenberg Institute and JARA-FIT, Forschungszentrum Jülich GmbH, Jülich, Germany

Amr H. H. Ramadan and Roger A. De Souza

Institute of Physical Chemistry (IPC) and JARA-FIT, RWTH Aachen University, Germany

Susanne Hoffmann-Eifert and Regina Dittmann

Peter Gruenberg Institute and JARA-FIT, Forschungszentrum Jülich GmbH, Jülich, Germany

We discuss electronic and ionic defect concentration profiles at the conducting interface between the two wide-band-gap insulators LaAlO$_3$ and SrTiO$_3$ (STO). The profiles are deduced from a thermodynamic model considering a local space charge layer (SCL) originating from charge transfer to the interface region, thus combining electronic and ionic reconstruction mechanisms. We show that the electrical potential confining the two-dimensional electron gas (2DEG) at the interface modifies the equilibrium defect concentrations in the SCL. For the n-conducting interface, positively charged oxygen vacancies are depleted within the SCL, while negatively charged strontium vacancies accumulate. Charge compensation within the SCL is achieved by a mixed ionic-electronic interface reconstruction, while the competition between 2DEG and localized ionic defects is controlled by ambient pO$_2$. The concentration of strontium vacancies increases drastically in oxidizing conditions and exhibits a steep depth profile towards the interface. Accounting for the low cation diffusivity in STO, we also discuss kinetic limitations of cation defect formation and the effect of a partial equilibration of the cation sublattice. We discuss the resulting implications for low temperature transport.

I. INTRODUCTION

The role of ionic defects in determining the electronic properties of LaAlO$_3$/SrTiO$_3$ (LAO/STO) interfaces and comparable systems has been a long-standing problem in the field of oxide interface electronics [1,2]. The main issue here is that the electronic interface reconstruction [3–5] and ionic defect-type reconstructions [6–10] have mostly been discussed separately. Typically, it is distinguished between the intrinsic, defect-free interface and the defective (oxygen-deficient) bulk of STO [6,7]. However, the intrinsic defect structure (forced by thermodynamic processes) in the interface region itself is often not considered.

Only a few reports discussed both electronic and ionic reconstructions in a common framework [11–15]. Current lattice disorder and defect chemistry models have already revealed the competition between charge compensation by electronic charge carriers forming the two-dimensional electron gas (2DEG) and charge compensation by acceptor-type ionic defects; in particular, strontium vacancies [9]. However, a model that unites electrostatic boundary conditions at the interface (charge transfer/polar catastrophe) and bulk defect chemistry describing the thermodynamic processes inside bulk STO is still missing. Furthermore, the nonzero local space charge at the interface has to be accommodated in a defect chemical framework. These issues will be addressed in this study.

It is generally established that a potential well forms at the LAO/STO interface, as a result of the potential buildup generated at the atomically abrupt interface of a perovskite with a polar surface, such as (100) LAO, and a perovskite with a nonpolar surface, such as (100) STO [3,16]. Various experimental and theoretical studies have shown that for the n-type interface electrons accumulate in a two-dimensional manner in this potential well [Figs. 1(a) and 1(b)]. The shape of the well is defined by the charge transfer from the LAO layer to the STO side of the interface as well as by the dielectric properties of STO.

For the conducting n-type interface, a negative charge $-Q/A$ is transferred into the STO, while a positive charge remains on the LAO side [17]. An important question here is how STO accommodates this negative charge.

In the conventional model of electronic reconstruction [1,3,18], the entire charge transfer is compensated by electrons forming the 2DEG. However, as oxides in general—and STO in particular—contain non-negligible concentrations of mobile, charged ionic defects [19], the potential formed at the LAO/STO interface and the associated electric field should affect not only electronic defects [band bending, Figs. 1(a)–1(c)], but *all* mobile, charged ionic defect species present in the bulk of STO [Figs. 1(d) and 1(e)]. In particular, at elevated temperatures such as growth or annealing temperatures—where the mobility of ionic species is drastically enhanced—ionic defect profiles are expected to align with the present electrostatic potential [15,20,21]. Thus, depending on their charge, ionic defects will be attracted or repulsed by the electric field at the interface.

Similar to electrons (holes), ionic defects carrying a negative (positive) charge will accumulate at (deplete from) the interface. In the particular case of STO, the relevant ionic defect species are positively charged oxygen vacancies, $V_O^{\bullet\bullet}$, which
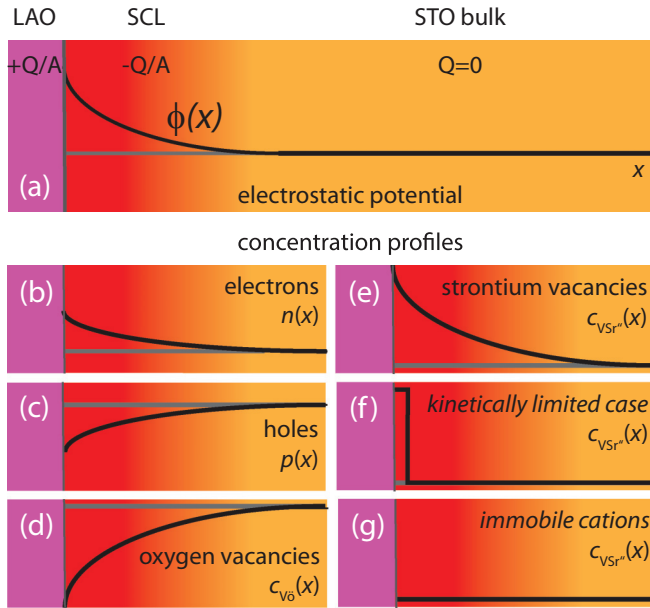
---

*gunkel@iwe.rwth-aachen.de

FIG. 1. Sketch of the space charge layer at the *n*-type LAO/STO interface. (a) Charge transfer drives a nonzero electrostatic potential, resulting in carrier accumulation [for electrons (b) and strontium vacancies (e) and (f)] or depletion [for holes (c) and oxygen vacancies (d)]. (b) and (c) correspond to classical band bending. (e)–(g) illustrate different scenarios for the strontium sublattice; equilibration throughout the entire SCL (e), kinetically limited equilibration confined to a narrow region close to the interface (f), and immobile strontium sublattice (g).

will thus be depleted from the *n*-type interface [Fig. 1(d)], and negatively charged strontium vacancies, V''_{Sr}, which will thus accumulate at the interface [Fig. 1(e)].

Equilibration of ionic defect profiles requires sufficiently fast diffusion of ions (vacancies) and thus takes place at elevated temperatures only. While oxygen vacancy diffusion is rapid at typical LAO/STO growth temperatures and lower [22], cation migration is much slower in STO [23,24]. Therefore, kinetic constraints may apply for the strontium vacancy equilibration process [Figs. 1(f) and 1(g)].

In this study, we present a model describing in detail the expected defect profiles established at the LAO/STO interface. Our model combines (1) the electrostatic bounds deduced from the charge transfer in the polar catastrophe picture and (2) the defect chemistry arising from thermodynamic processes in the bulk of STO. It hence represents a unified model, considering both defect formation processes (driven by energy and entropy) and electrostatics.

The results indicate that charge transfer into the interface is the underlying doping mechanism at the LAO/STO interface. As a result, a thermally stable, mixed electronic-ionic defect profile is established within the space charge layer (SCL). Depending on ambient conditions the negative charge density in the *n*-type SCL is accommodated by electrons and acceptor-type strontium vacancies. The balance between 2DEG and ionic defects is controlled by pO_2. We find an electron gas that is confined mainly within $\lesssim 5$–10 nm from the interface. The concentration of strontium vacancies scales on a similar length scale. The results emphasize that strontium vacancy formation

at the interface is essentially important to explain the 2DEG's low carrier density found in LAO/STO after oxidation.

II. LATTICE DISORDER AND DEFECT CHEMISTRY OF BULK STO

First, the bulk defect concentrations in STO have to be determined. Commonly, STO single crystals are used as substrate material for LAO/STO heterostructures. These single crystals typically have an effective acceptor-type impurity level ($c_{A'}$) of about 10–100 ppm [21,25,26]. Hence, nominally undoped STO substrates have to be treated as weakly acceptor-doped material.

The equilibrium bulk defect concentrations, c_{def}^b, of the relevant defects species, electrons (n^b), electron holes (p^b), oxygen vacancies ($c_{V_O^{\bullet\bullet}}^b$), and strontium vacancies ($c_{V''_{Sr}}^b$) can (in agreement with experiment) be calculated as a function of temperature, T, and oxygen partial pressure, pO_2 [19,21,25–27].

For this study, we considered a temperature of 950 K (a typical growth temperature for LAO/STO) and $c_{A'} \approx 10^{17}$ cm^{-3} (a typical impurity doping level for STO). The resulting bulk defect concentrations as a function of pO_2 are shown in Supplemental Material Fig. S1 [28]. These values serve as boundary conditions for the calculations of the space charge potential at the LAO/STO interface.

III. MODELING OF THE INTERFACE SCL

A. Thermodynamic processes in SCLs

At elevated temperatures, such as during growth or annealing, ionic defects are mobile charge carriers that—given sufficient time—will align with the local electrostatic potential. This leads in the equilibrium state to defect concentrations within the SCL differing drastically from their bulk values. The equilibrium condition corresponds to the gradient in the electrochemical potential of a mobile defect being zero (i.e., minimum Gibbs' energy).

We consider the standard form of the electrochemical potential, which includes not only the standard formation energy of a defect, g_{def}, but also terms relating to the configurational entropy and the electrostatic potential

$$\eta_{def} = g_{def} + k_B T \ln\left(\frac{c_{def}(x)}{N_{def} - c_{def}(x)}\right) + z_{def} e \phi(x). \quad (1)$$

Here, $c_{def}(x)$ denotes the concentration of the defect "def" = $\{n, p, V_O^{\bullet\bullet}, V''_{Sr}\}$ at the distance x from the interface, z_{def} the defect's charge number, e the elementary charge, $\phi(x)$ the electrostatic potential, and N_{def} the number of available lattice sites per volume. For electrons (holes), N_{def} corresponds to the effective density of states at the conduction (valence) band edge [21,25].

In general, g_{def} may depend on the distance from the interface [21,27,29]. However, the resulting thermodynamic driving forces, such as observed at the surface of STO [27], usually cause only weak carrier accumulation not sufficient to force the formation of a high density electron gas. For the sake of simplicity, we will therefore treat g_{def} as distance independent.

Far away from the interface, the defect concentrations are given by the potential-free bulk concentrations [$c_{\mathrm{def}}(\infty) = c_{\mathrm{def}}^{\mathrm{b}}$] obtained in the previous section. In equilibrium, η_{def} is constant throughout the entire system for every defect species. Using $\eta_{\mathrm{def}}(x) - \eta_{\mathrm{def}}(\infty) = 0$, this yields a local defect concentration of

$$c_{\mathrm{def}}(x) = \frac{c_{\mathrm{def}}^{\mathrm{b}} \exp[-z_{\mathrm{def}} e\phi(x)/k_{\mathrm{B}}T]}{1 + \frac{c_{\mathrm{def}}^{\mathrm{b}}}{N_{\mathrm{def}}}\{\exp[-z_{\mathrm{def}} e\phi(x)/k_{\mathrm{B}}T] - 1\}} \quad (2)$$

in the presence of a nonzero electrostatic potential. (Here, we set arbitrarily $\phi(\infty) = 0$ in the bulk of STO [30].) Due to the low mobility of V_{Sr}'' in STO, the equilibration of the strontium sublattice at typical growth temperatures is likely to be kinetically limited. In other words, it is not necessarily clear that a full equilibrium is reached within a reasonable time scale. Therefore, Eqs. (1) and (2) may not hold for the case "def" = V_{Sr}''. The effect of this limitation will be discussed comprehensively in Sec. VI.

B. Charge transfer at the LAO/STO interface

In order to accommodate the particular properties of the LAO/STO interface one has to consider boundary conditions specific to this problem. In particular, the polar catastrophe forces charge transfer into the interface defining the electric field established at $x = 0$. According to Gauss' law, the electric field, $E = -d\phi/dx$, at the interface is given by

$$\epsilon_{\mathrm{r}}\epsilon_0 \frac{d\phi}{dx}\bigg|_{x=0} = -Q/A, \quad (3)$$

where $-Q/A$ denotes the charge per area transferred on the STO side of the interface, $\epsilon_{\mathrm{r}}(T)$ the temperature-dependent dielectric constant [31], and ϵ_0 the vacuum permittivity.

The charge transfer according to the polar catastrophe picture ($Q/A = 3.2 \times 10^{14}\ e\ \mathrm{cm}^{-2}$ [1,3]) may be diminished, e.g., by structural distortions [32], polarization of the crystal lattice [33], and nonstoichiometry of the LAO thin film [34,35] reducing Q/A. Therefore, without affecting the general validity of the model, we use the charge value obtained

directly from high temperature equilibrium experiments, $Q/A \approx 1 \times 10^{14}\ e\ \mathrm{cm}^{-2}$ [9,36], which is slightly lower than the proposed value. This charge is associated with an interfacial electric field of $E(0) = 1.8 \times 10^6$ V/cm at 950 K and drives the formation of the SCL.

In order to calculate $\phi(x)$, one has to consider Poisson's equation

$$-\epsilon_{\mathrm{r}}\epsilon_0 \frac{d^2\phi(x)}{dx^2} = \rho(x) = e\Big[-c_{\mathrm{A}'} + \sum z_{\mathrm{def}} c_{\mathrm{def}}(x)\Big]. \quad (4)$$

Here, it is assumed that ϵ_{r} is field independent, $d\epsilon_{\mathrm{r}}/dx = 0$, which is valid at elevated temperatures [37,38].

In Eq. (4), the charge density ρ implicitly depends on the potential $\phi(x)$ via $c_{\mathrm{def}}(x)$ [Eq. (2)]. Moreover, all ionic and electronic charges are considered to contribute to ρ, while previous models assumed electrons to be the only charge carrier within the SCL [39–41]. In particular, here we consider the strontium sublattice to achieve thermodynamic equilibrium and to contribute to ρ. The impurity concentration $c_{\mathrm{A}'}$ in the bulk of STO contributes as a constant background doping term [42].

Adding the boundary condition that the bulk of STO is field-free (i.e., $\frac{d\phi}{dx}|_{x=\infty} = 0$) the electrostatic problem is fully defined and $\phi(x)$ can be calculated in a self-consistent numerical manner as a function of $p\mathrm{O}_2$ and T.

IV. RESULTS OF MODEL CALCULATIONS

Figure 2 shows the resulting depth profiles of the electrostatic potential (a), electric field (b), and charge density (c) in the SCL as a function of distance x from the interface. The calculations were carried out for $T = 950$ K. Hence, $\phi(x)$ corresponds to the space charge potential established at the LAO/STO interface in high temperature equilibrium, e.g., at growth or annealing conditions. The oxygen partial pressure was varied between $-23 < \log(p\mathrm{O}_2/\mathrm{bar}) < 0$.

The width of the SCL varies between 200 nm at $p\mathrm{O}_2 = 1 \times 10^{-23}$ bar and 400 nm at $p\mathrm{O}_2 = 1$ bar. At distances above 50 nm from the interface ρ is essentially constant
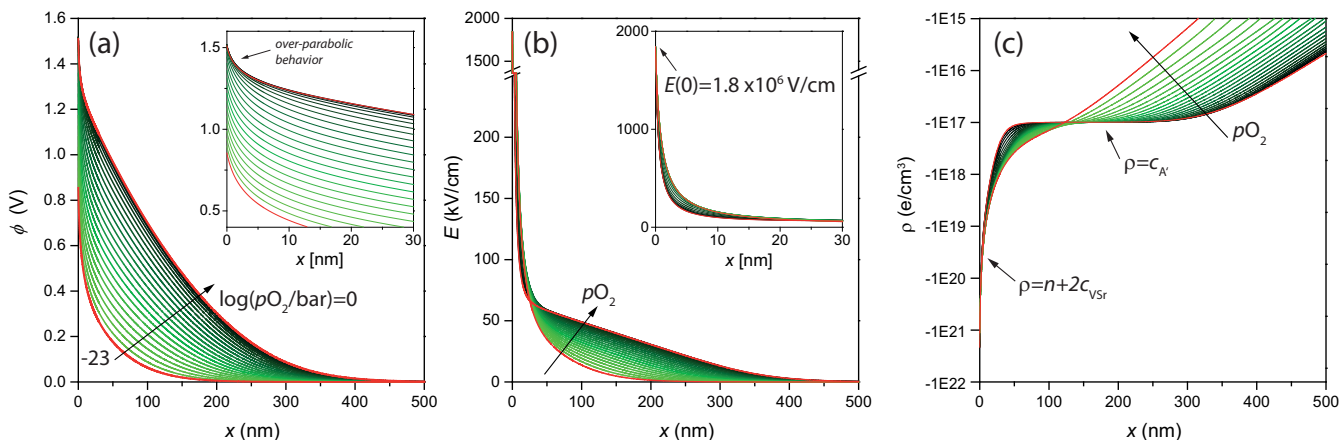

FIG. 2. (a) Space charge potential obtained at $T = 950$ K for oxygen pressures between 1 bar and 10^{-23} bar. For the highest and lowest $p\mathrm{O}_2$, $\phi(x)$ is plotted as a red line, and for intermediate pressures the color changes from green to black with increasing $p\mathrm{O}_2$. Inset: Potential profile in the near-interface region. (b) Corresponding electric field within the SCL. Inset: Field behavior in the near-interface region. (c) Charge density distribution, ρ, within the SCL. For these calculations, full equilibration of the strontium sublattice was considered.

and given by $c_{A'}$ [Fig. 2(c)]. In this range, ϕ varies in a parabolic manner (and E in a linear manner) such as known from classical semiconductor physics [43]. We term this a Mott-Schottky-type SCL, as it results from a depletion of the (bulk) majority carriers, $V_O^{\bullet\bullet}$, within the SCL. The SCL vanishes in the bulk (as $2c_{V_O^{\bullet\bullet}}$ approaches $c_{A'}$; cf. Fig. S2 [28]).

As one approaches the interface ($x \lesssim 5$–10 nm), the potential increases in an overparabolic manner [see inset of Fig. 2(a)] reaching interface potentials of $\phi(0) = 1.5$ V at $pO_2 = 1$ bar and 0.8 V at $pO_2 = 1 \times 10^{-23}$ bar. This region reflects the actual 2D potential well established at the LAO/STO interface.

Within this sharp well, $\phi(x)$ typically drops by about 0.2–0.3 V, while the electrical field drops by about one order of magnitude [Fig. 2(b)]. The space charge is generated by mobile defect species, which vary quickly within this region [cf. Fig. 2(c)]. It thus corresponds to a Debye-type charge compensation. As we will see below, depending on pO_2 the dominant mobile charge carriers are either electrons or strontium vacancies or both.

The pO_2 dependence of the potential is related to the pO_2-dependent bulk defect concentrations $c_{\mathrm{def}}^{\mathrm{b}}$. Note that as a result of bulk defect chemistry this bound varies only in n^{b} (and p^{b}) when varying the pO_2, while the ionic defect concentrations $c_{V_O^{\bullet\bullet}}^{\mathrm{b}}$ and $c_{V_{Sr}''}^{\mathrm{b}}$ remain essentially unchanged in the bulk. Hence, while the ionic defect structure within the SCL varies strongly, the amount of ionic defects formed/annihilated in the bulk STO is negligible [see Fig. S1 [28]].

The resulting defect concentration profiles in the SCL are shown in detail in supplementary Fig. S2 for selected pO_2 [28]. As a major result, we find that electron holes and $V_O^{\bullet\bullet}$ are strongly depleted in the SCL, while electrons and V_{Sr}'' accumulate, as expected for the n-type interface.

The behavior of the accumulated defect species, electrons, and V_{Sr}'' in the Debye-type region is most interesting with respect to electron transport at the interface. Figure 3 shows

$n(x)$ as well as $c_{V_{Sr}''}(x)$ in the near-interface region ($x \lesssim 30$ nm) for various pO_2. Both concentration profiles show a sharp upturn close to the interface associated with the sharp upturn observed already in $\phi(x)$ [inset of Fig. 2(a)].

Typically, $n(x)$ drops by more than one (two) order(s) of magnitude within about 5 (10) nm from the interface. Hence, about 99% of the electrons are confined to this region, in good agreement with previous reports [3,5,39,40,44]. Further inside the STO, $n(x)$ decays slowly towards its bulk value following the Mott-Schottky-type behavior (cf. Fig. S2 [28]). Starting from reducing conditions, $n(x)$ changes only slightly when increasing pO_2 (black arrow). In oxidizing conditions, however, the electron profile is significantly shifted downwards and slightly widens [$n(x)$ drops by two orders of magnitude at 22 nm].

$c_{V_{Sr}''}(x)$ shows the opposite dependence on pO_2. While the concentration of V_{Sr}'' is negligible at low pO_2, $c_{V_{Sr}''}(x)$ increases constantly with increasing pO_2 (red arrow) finally reaching concentrations comparable to and even superior to $n(x)$.

In oxidizing conditions, $\langle c_{V_{Sr}''} \rangle$ (1 uc) reaches about 6×10^{20} cm^{-3} corresponding to about 3.5 at. % of vacant cation sites averaged over the first STO unit cell ($0 < x/\mathrm{nm} < 0.4$). Proceeding into the bulk, $c_{V_{Sr}''}(x)$ drops quickly below the 10–100 ppm level after a few nanometers. In the near-interface region, charge compensation is thus accomplished by both electrons *and* strontium vacancies [$\rho(x) = n(x) + 2c_{V_{Sr}''}(x)$; cf. Fig. 2(c)].

For clarity, we plot in Fig. 3(b) $n(x)$ and $c_{V_{Sr}''}(x)$ in the near-interface region for selected pO_2. At moderately low $pO_2 = 1 \times 10^{-10}$ mbar, $c_{V_{Sr}''}(x)$ is negligible. Hence, charge compensation is fully electronic corresponding to the generally assumed electronic interface reconstruction. At typical growth pressure ($pO_2 = 1 \times 10^{-4}$ mbar), however, $c_{V_{Sr}''}(x)$ becomes more significant taking similar values as $n(x)$ close to the interface. Hence, in this environment our model delivers a mixed electronic-ionic interface reconstruction, yet with negligible effect on $n(x)$. For annealing pressure ($pO_2 = 1000$ mbar), $c_{V_{Sr}''}(x)$ increases further, while $n(x)$ is significantly reduced. Thus, the interface reconstruction becomes rather ionic, while an electron gas with reduced carrier density remains in general agreement with transport measurements on post-annealed LAO/STO samples [2,4].

V. COMPARISON WITH EXPERIMENTAL DATA

Transport experiments on LAO/STO yield the sheet electron density n^{s}. We can obtain this quantity from our simulations according to $c_{\mathrm{def}}^{\mathrm{s}} = \int_0^\infty c_{\mathrm{def}}(x)dx$. In this manner we can compare our simulation results directly with published experimental data.

In Fig. 4(a), we plot the sheet electron density as well as the sheet concentration of strontium vacancies for an equilibration temperature of 950 K. In reducing atmospheres, n^{s} is constant at a value of 1×10^{14} cm^{-2}, which corresponds to the amount of charge transferred into the interface (as assumed for these model calculations), $n^{\mathrm{s}} = Q/eA$. At the same time, $c_{V_{Sr}''}^{\mathrm{s}}$ takes negligibly low values, confirming that charge
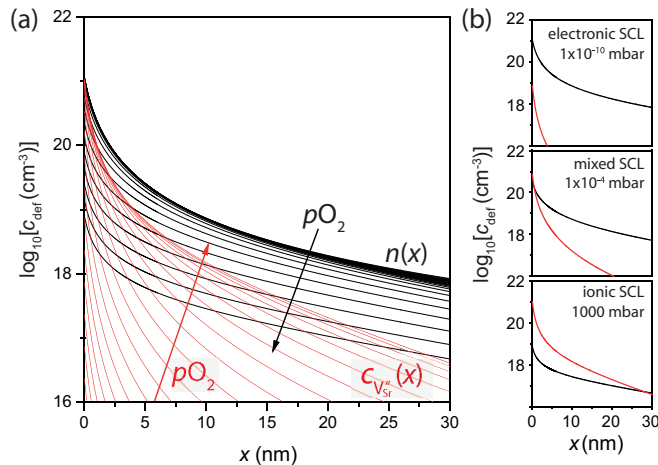

FIG. 3. (a) Profiles of accumulated defect species, electrons (black) and strontium vacancies (red), resulting from the space charge potential established at the LAO/STO interface for $-23 < \log(pO_2/\mathrm{bar}) < 0$, considering full equilibration of the strontium sublattice. (b) Electron (black) and strontium vacancy (red) profiles in the near-interface region for dedicated oxygen pressures.
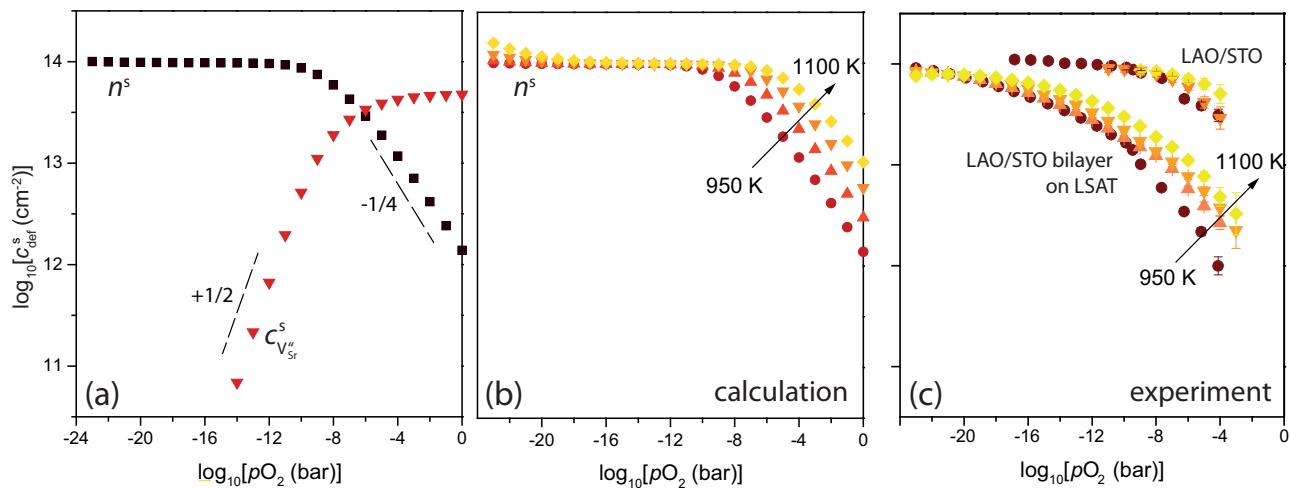
FIG. 4. Sheet defect concentrations obtained by integration over the SCL, considering the fully equilibrated strontium sublattice. (a) Sheet electron concentration, n^s, and sheet concentration of strontium vacancies, $c_{V_{Sr}''}^s$, obtained at an equilibration temperature of 950 K. (b) n^s obtained at various temperatures between 900 and 1100 K (typical growth and annealing temperatures for LAO/STO). The activation energy in oxidizing atmosphere is 1.2 eV. (c) Experimental data obtained for LAO/STO and LAO/STO/LSAT heterostructures. Details are discussed in Ref. [9].

compensation is accomplished by electrons only (electronic reconstruction [1,3]).

In more oxidizing conditions, n^s decreases below Q/eA, while $c_{V_{Sr}''}^s$ rises and finally saturates at a value $c_{V_{Sr}''}^s = Q/2eA$. This corresponds to ionic compensation of the transferred charge. In fact, as strontium vacancies accomplish charge compensation, the electron density can be reduced while maintaining the validity of the electrostatic boundary conditions given for the LAO/STO interface. The remaining sheet electron density in oxidizing conditions ranges from 10^{12} cm^{-2} to a few times 10^{13} cm^{-2}. Thus, depending on actual (annealing) temperature and gas mixture, the resulting carrier density should vary in this range which is in good agreement with experimental observations [2,4]. Our model can thus explain why the carrier densities typically observed for LAO/STO are often well below the value expected from the polar catastrophe picture.

For intermediate pO_2 values in the growth pressure regime, both sheet concentrations take comparable values corresponding to a mixed ionic-electronic compensation of charge. The sheet concentrations determined here show a very similar behavior as the bulk concentrations in donor-doped STO [11,19,25,36]. While n^s is constant in reducing atmosphere, $c_{V_{Sr}''}^s$ increases as $pO_2^{1/2}$. While $c_{V_{Sr}''}^s$ is constant in oxidizing conditions, n^s decreases as $pO_2^{-1/4}$ [9].

In Fig. 4(b), n^s is shown for various temperatures. The plateaulike region observed in reducing atmosphere is temperature independent, while n^s shows a temperature activated behavior in the region of ionic compensation. The activation energy in this region is about 1.2 eV.

At very low pressure ($pO_2 \lesssim 10^{-20}$ bar) and the highest considered temperatures ($T > 1000$ K), n^s shows an additional increase. This behavior corresponds to the intrinsic behavior of the bulk of STO. Here, the equilibrium bulk concentration of oxygen vacancies increases above the ac-

ceptor level ($n = 2c_{V_O^{\bullet\bullet}}^b > c_{A'}$; cf. Fig. S1) and one obtains bulk behavior as the result of parallel conduction in the substrate.

The behavior obtained from the SCL model is fully consistent with the experimental data obtained from high temperature equilibrium conductance measurements on different LAO/STO heterostructures [Fig. 4(c)] as discussed in detail in Refs. [9,36]. Experimental data can only be obtained in a limited pO_2 range, as the measurement is affected by the substrate contribution. Nevertheless, a comparison of Figs. 4(b) and 4(c) reveals that the dependence on pO_2 as well as the temperature dependence obtained in the model calculations is in good agreement with experiment. In particular, an activation energy of 1.0 eV has been found experimentally [9] for the LAO/STO interface, which is remarkably similar to the value obtained in our model calculations. In contrast, the activation energy measured in the bulk of donor-doped bulk STO [2.5 eV [25]] is significantly larger. We can therefore conclude that this reduced activation energy is the result of the electrostatic potential in the SCL at the LAO/STO interface modifying the ionic defect concentrations. Moreover, we can specify that the donor-type conduction mechanism is a result of the electrostatic bounds at the LAO/STO interface. The charge transfer introduces a SCL at the interface, with modified electronic and ionic structure and thus a modified defect chemistry.

The experiments furthermore revealed a shift of the entire characteristic towards lower pO_2 when turning from STO single crystal samples to LAO/STO bilayer samples [see Fig. 4(c) and Ref. [9]]. This shift can be understood in terms of an increased defect density in the bulk of the STO thin film incorporated during growth [11]. Consistently, in our model, an increase of $c_{A'}$ to a few atomic percent reproduces a similar shift of the characteristic.

Note that for the entire modeling we have used thermodynamic and dielectric data collected directly from
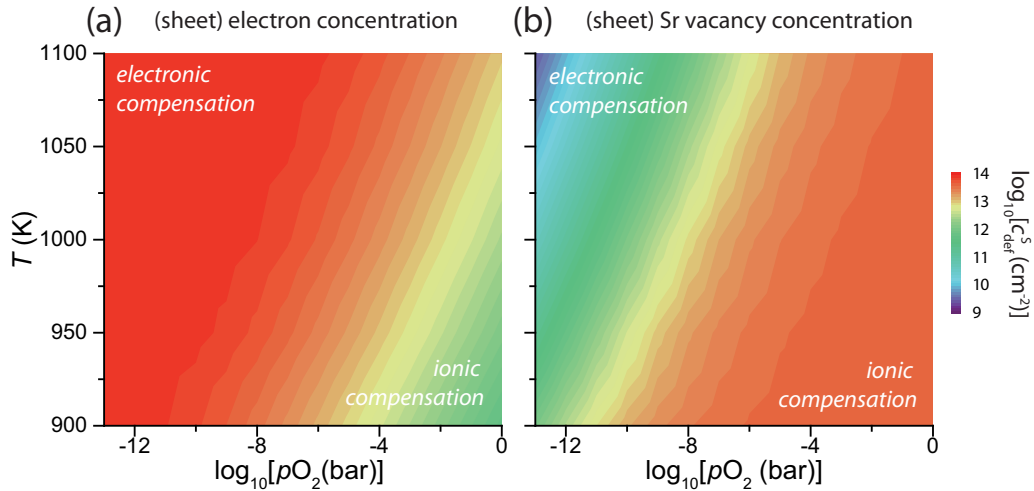
FIG. 5. False color plot of (a) sheet electron concentration and (b) sheet Sr vacancy concentration obtained from the model calculations as a function of temperature and ambient $p\text{O}_2$.

experiments (see Supplemental Material, Sec. I [28]) or from the literature. The only parameters varied here are the reaction constants of the bulk Schottky equilibrium which essentially determines the bulk concentration of V_{Sr}'' in equilibrium (cf. Fig. S1) [45].

Moreover, the SCL model naturally returns an insulating p-type interface where the now positive space charge $(+Q/A)$ is accomplished by oxygen vacancies, which is consistent with previous reports [3,46]. The p-type interface is discussed in more detail in the Supplemental Material (Figs. S3 and S4 [28]).

In order to summarize the results of this section, we plot in Fig. 5 the sheet concentrations of electrons (a) and Sr vacancies (b) obtained at a given T and $p\text{O}_2$ in a false color plot. The inverse color gradients in (a) and (b) illustrate the transition between electronic and ionic charge compensation at the LAO/STO interface depending on ambient conditions. Electronic charge compensation is favored at increased T and/or lowered $p\text{O}_2$, while ionic charge compensation is favored at lower T and/or increased $p\text{O}_2$.

VI. KINETIC LIMITATIONS OF THE V_{Sr}'' FORMATION PROCESS

In the foregoing sections, we have assumed that the strontium sublattice reaches an equilibrium within the SCL formed at the LAO/STO interface. This, however, requires sufficiently fast diffusion of V_{Sr}'' on the length scale of a few hundred nanometers (cf. Fig. S2 [28]). However, the self-diffusion coefficient for V_{Sr}'' is rather low [23]. Therefore, even though the strontium vacancy diffusion may be accelerated by barrier lowering and drift due to the electric field in the SCL [47,48], the V_{Sr}'' diffusion length may be only in the range of a few nanometers (in a couple of hours at 950 K). Thus, the strontium sublattice may be in thermodynamic equilibrium only within a narrow region at the interface, rather than within the entire space charge layer. This kinetic limitation for the strontium sublattice is discussed in the following on the basis of two limiting cases.

A. Immobile cation sublattice

In this scenario, we consider V_{Sr}'' not to equilibrate at all with the potential at any given ambient conditions, i.e., $c_{\text{V}_{\text{Sr}}''}(x) = c_{\text{V}_{\text{Sr}}''}^{\text{b}}$ for all x [Fig. 1(g)]. In this case, $c_{\text{V}_{\text{Sr}}''}$ has only negligible effect on the charge density within the SCL [Eq. (2)].

Figure 6(a) shows the electron density established at the LAO/STO interface at 950 K for various oxygen partial pressures $[-23 \, (\text{red}) < \log(p\text{O}_2/\text{bar}) < 0 \, (\text{black})]$. Clearly, the electron density in the near-interface region is $p\text{O}_2$ independent, since the electric field at the interface is merely compensated by electrons at any $p\text{O}_2$.

Similarly, the sheet electron density [Fig. 6(b)] neither shows any dependence on $p\text{O}_2$ nor on T. This behavior clearly differs from the experimentally determined sheet electron density [Fig. 4(c)]. In particular, the decrease in n^{s} observed in oxidizing conditions is absent due to the lack of alternative charge compensating defects in the SCL. Hence, one can clearly conclude that ionic charge compensation by V_{Sr}'' in addition to electronic compensation is mandatory to explain the experimentally observed behavior.

B. Kinetically limited V_{Sr}'' formation

As a second limiting case, we discuss a scenario in which the strontium sublattice equilibrates only within a single unit cell at the interface. For $0 < x < 0.4$ nm, we use Eq. (2) to determine the strontium vacancy concentration at the interface, while $c_{\text{V}_{\text{Sr}}''}(x) = c_{\text{V}_{\text{Sr}}''}^{\text{b}}$ anywhere else in the SCL, so that $c_{\text{V}_{\text{Sr}}''}(x)$ takes a boxlike shape [Fig. 1(f)]. Hence, at the interface itself a fraction of the transferred charge can be compensated by ionic defects.

Figure 7(a) shows the resulting electron concentrations obtained at 950 K for various $p\text{O}_2$ $[-23 \, (\text{yellow}) < \log(p\text{O}_2/\text{bar}) < 0 \, (\text{black})]$. The gray bars indicate the mean concentration of strontium vacancies in the first unit cell at the interface. For better visibility, the interfacial concentration of V_{Sr}'' is enlarged on the left-hand side of Fig. 7(a).

In this scenario, we find again an increasing concentration of V_{Sr}'' with increasing $p\text{O}_2$, which in oxidizing conditions
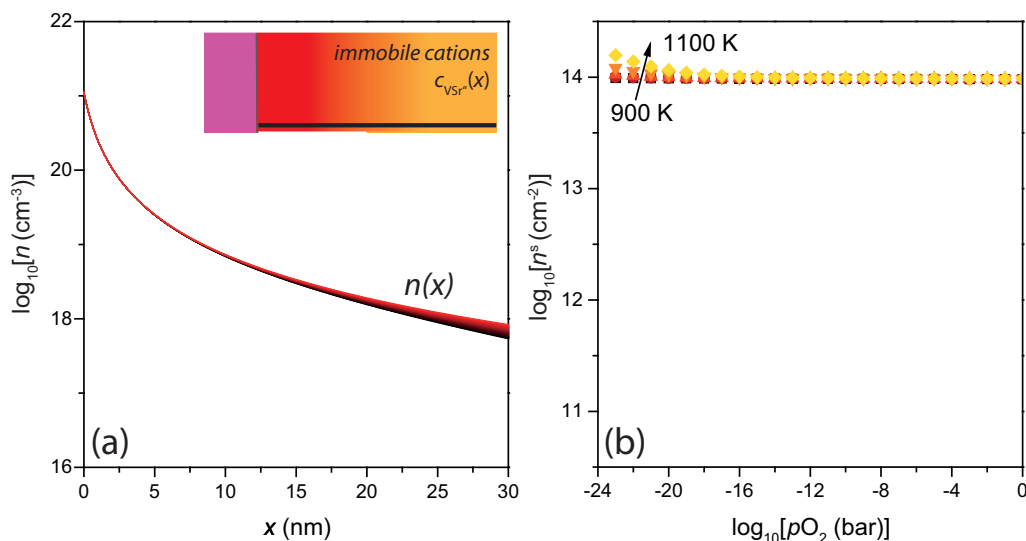
FIG. 6. Electron concentrations calculated for the LAO/STO interface assuming an immobile cation sublattice. (a) Electron concentration profiles, $n(x)$, at an equilibration temperature of 950 K [-23 (red) $< \log(pO_2/\text{bar}) < 0$ (black)]. (b) n^s obtained by integration over the SCL at various temperatures between 900 and 1100 K.

exceeds the maximum electron concentration within the SCL. Thus, in the kinetic limit, we observe a similar transition from purely electronic compensation to mixed ionic-electronic compensation to mainly ionic compensation when traversing from reducing to oxidizing conditions. At maximum, $c^b_{V''_{Sr}}$ takes values up to about 1×10^{21} cm^{-3} corresponding to about 6 at. % for $pO_2 = 1$ bar.

The electron profiles vary only slightly in reducing and intermediate atmospheres (yellow-red), while they shift sig-nificantly downwards and widen [$n(x)$ drops to 1% at ≈ 30 nm] in oxidizing conditions.

Figure 7(b) shows the resulting sheet carrier density obtained in the interface region obtained by integration of the electron density profiles across the SCL. Similar to Fig. 4(b), we find a plateaulike, temperature-independent n^s in reducing and intermediate conditions, while n^s decreases in oxidizing conditions and becomes temperature activated, thus recovering the characteristic feature of ionic charge compensation discussed in Sec. IV. While the decrease of
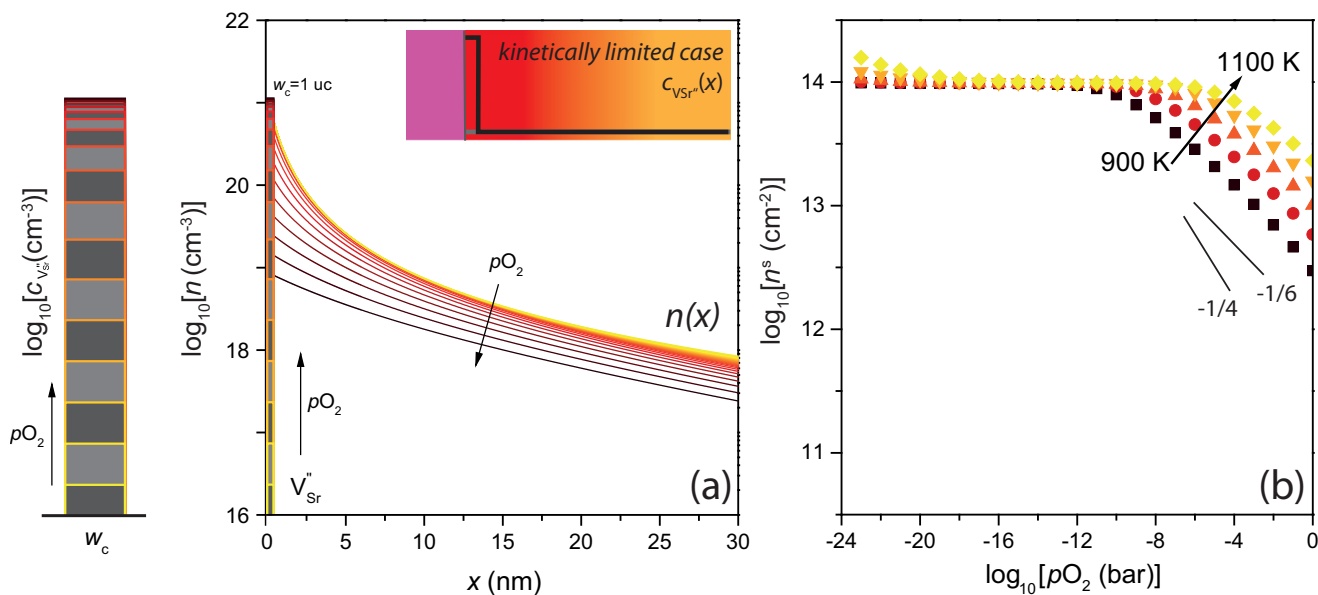

FIG. 7. Electron concentrations calculated for the LAO/STO interface assuming a kinetically limited equilibration of the strontium sublattice. V''_{Sr} are assumed to equilibrate only within a narrow region at the interface ($w_c = 1$ uc). (a) Electron concentration profiles, $n(x)$, at 950 K [-23 (yellow) $< \log(pO_2/\text{bar}) < 0$ (black)]. $c^b_{V''_{Sr}}$ at the interface is illustrated in an enlarged view on the left-hand side of the figure. (b) n^s obtained in the kinetic limit for various temperatures between 900 and 1100 K.

n^s in oxidizing conditions becomes slightly weaker than for full equilibration of the cation sublattice, the general behavior is rather similar and consistent with the experimental data [Fig. 4(c)]. Hence, we conclude that Sr vacancy formation at least in a narrow region close to the interface is essential to understand the 2DEG electron density established at the LAO/STO interface in oxidizing conditions.

This treatment of a kinetically limited cation sublattice may be oversimplified, as cation diffusion physically does take place in the course of time. In fact, cation diffusion should be facilitated in the SCL compared to the bulk as a result of the electric field. As a result of inwards diffusion of V_{Sr}'', case *B* discussed here will converge into the case of full equilibration in the course of time. For the real defect structure established at the LAO/STO interface, it is therefore reasonable to assume a case between scenario *B* and the scenario of full equilibration (discussed in Sec. IV). Hence, the V_{Sr}'' profiles are expected to be even steeper than the ones presented in Fig. 3. The kinetic limitations of the strontium sublattice hence further confine ionic defects to the very-near-interface region. Note again, that neglecting any contribution of V_{Sr}'' (case *A*) is evidently not sufficient to explain the experimental data at all.

VII. IMPLICATIONS FOR LOW TEMPERATURE TRANSPORT

As indicated above, our model correctly predicts how the interfacial carrier density varies with ambient pO_2 as observed after oxygen annealing. The proposal of electronic trap states at the interface, such as considered in the literature [41,49], may now be reexamined in the light of including ionic defects. The formation of V_{Sr}'' results in the annihilation of electrons, and this effectively produces similar behavior to that of electronic interface states. However, the underlying physical process is fundamentally different.

Moreover, the steep defect concentration profiles at the interface cause a strongly inhomogeneous system. As a result, depending on thermodynamic bounds, such as oxygen pressure and temperature during growth, one expects an electron gas with specific structure that may also affect the resulting interface properties (e.g., electron mobility, superconductivity, magnetism [2,50–53]). Moreover, electrons are expected to exhibit a mobility that varies with x, $\mu_n = \mu_n(x)$. As a result, one may expect a complex (nonlinear) behavior of the Hall resistance at low temperature—caused by an inhomogeneous defect structure in addition to the specific band structure at the interface [54,55]. Considering V_{Sr}'' as most important scattering centers, the electron mobility should decrease with increasing growth pressure such as observed in Refs. [2,56].

While the steep ionic defect profiles established at growth temperatures are frozen at low temperature and do not change upon cooling, $n(x)$ will adopt the drastically enhanced dielectric constant of STO at low temperature. Thus, electrons leak into the region further inside the SCL, where $c_{V_{Sr}''}$ is drastically reduced (in particular in a kinetically limited case, Fig. 7). As a result, one may still observe considerably high electron mobilities in annealed samples exhibiting a dilute 2DEG with reduced carrier density.

High concentrations of defects close to the interface may also explain the low mobility observed in LAO/STO bilayers

and superlattices [11,57,58] as the 2DEG is confined to the interface-near, defective region.

Finally, our model predicts a route for enhancing the electron mobility at polar/nonpolar oxide interfaces. Lowering the charge transfer into the interface is expected to suppress the formation of V_{Sr}'' in oxidizing conditions (where $c_{V_{Sr}''}^s = Q/2eA$). In this view, the use of low-polarity materials, such as in $(La,Sr)(Al,Ta)O_3/STO$ (LSAT/STO [59]), is expected to be beneficial for the interfacial electron mobility, classically scaling inverse proportional with defect density.

Moreover, V_{Sr}'' formation may be suppressed by avoiding high-temperature treatments. Therefore, STO-based 2DEGs obtained by room-temperature layer growth [60–62] or by ionic-liquid gating [63–65] may exhibit increased electron mobility, too.

VIII. CONCLUSIONS

We presented electronic and ionic defect concentration profiles at the LAO/STO interface resulting from a thermodynamic treatment with electrostatic boundary conditions deduced from the charge transfer into the interface.

Our model merges the polar catastrophe picture with the classical defect chemistry of bulk STO. It identifies the charge transfer into the interface as a donor-type doping mechanism in LAO/STO heterostructures in a defect chemical framework. The deduced defect concentration profiles are the result of thermodynamic considerations reflecting the effects of energetics (electrostatics, band bending, and defect formation energies), entropy, and kinetics.

It is found for the *n*-type interface that there is a competition of electrons and strontium vacancies both accumulating in the space charge layer at the interface. Oxygen vacancies (and electron holes) are depleted within the *n*-type SCL.

The balance of electronic and ionic charge compensation is controlled by pO_2. Ionic compensation becomes more and more significant in high oxygen pressures. Thus, the *intrinsic* defect structure established at the LAO/STO interface depends on the ambient conditions during growth and during post-deposition annealing processes.

Reflecting the 2D character of the system, the electron profiles are very steep within the first 10 nm from the interface, containing about 99% of the total electron concentration. The strontium vacancy profile scales on a similar length scale. The kinetic limitations of strontium diffusion at typical growth and annealing conditions promote a strontium vacancy profile that is even steeper and more confined than the electron profile. This inhomogeneous ionic-electronic defect structure at the interface yields complex transport properties in the low temperature regime where the electron mobility is expected to depend on the distance from the interface.

[1] A. Ohtomo and H. Y. Hwang, Nature (London) **427**, 423 (2004).

[2] A. Brinkman, M. Huijben, M. V. Zalk, J. Huijben, U. Zeitler, J. C. Maan, W. G. V. der Wiel, G. Rijnders, D. H. A. Blank, and H. Hilgenkamp, Nat. Mater. **6**, 493 (2007).

[3] N. Nakagawa, H. Y. Hwang, and D. A. Muller, Nat. Mater. **5**, 204 (2006).

[4] S. Thiel, G. Hammerl, A. Schmehl, C. W. Schneider, and J. Mannhart, Science **313**, 1942 (2006).

[5] M. Sing, G. Berner, K. Goß, A. Müller, A. Ruff, A. Wetscherek, S. Thiel, J. Mannhart, S. A. Pauli, C. W. Schneider, P. R. Willmott, M. Gorgoi, F. Schäfers, and R. Claessen, Phys. Rev. Lett. **102**, 176805 (2009).

[6] W. Siemons, G. Koster, H. Yamamoto, T. H. Geballe, D. H. A. Blank, and M. R. Beasley, Phys. Rev. B **76**, 155111 (2007).

[7] G. Herranz, M. Basletic, M. Bibes, C. Carretero, E. Tafra, E. Jacquet, K. Bouzehouane, C. Deranlot, A. Hamzic, J. M. Broto, A. Barthelemy, and A. Fert, Phys. Rev. Lett. **98**, 216803 (2007).

[8] P. R. Willmott, S. A. Pauli, R. Herger, C. M. Schlepütz, D. Martoccia, B. D. Patterson, B. Delley, R. Clarke, D. Kumah, C. Cionca, and Y. Yacoby, Phys. Rev. Lett. **99**, 155502 (2007).

[9] F. Gunkel, P. Brinks, S. Hoffmann-Eifert, R. Dittmann, M. Huijben, J. E. Kleibeuker, G. Koster, G. Rijnders, and R. Waser, Appl. Phys. Lett. **100**, 052103 (2012).

[10] S. A. Pauli, S. J. Leake, B. Delley, M. Björck, C. W. Schneider, C. M. Schlepütz, D. Martoccia, S. Paetel, J. Mannhart, and P. R. Willmott, Phys. Rev. Lett. **106**, 036101 (2011).

[11] F. Gunkel, S. Wicklein, S. Hoffmann-Eifert, P. Meuffels, P. Brinks, M. Huijben, G. Rijnders, R. Waser, and R. Dittmann, Nanoscale **7**, 1013 (2015).

[12] V. Vonk, J. Huijben, D. Kukuruznyak, A. Stierle, H. Hilgenkamp, A. Brinkman, and S. Harkema, Phys. Rev. B **85**, 045401 (2012).

[13] Z. Zhong, P. X. Xu, and P. J. Kelly, Phys. Rev. B **82**, 165127 (2010).

[14] L. Yu and A. Zunger, Nat. Commun. **5**, 5118 (2014).

[15] F. Baiutti, G. Logvenov, G. Gregori, G. Cristiani, Y. Wang, W. Sigle, P. A. van Aken, and J. Maier, Nat. Commun. **6**, 8586 (2015).

[16] J. Mannhart, D. Blank, H. Hwang, A. Millis, and J.-M. Triscone, MRS Bull. **33**, 1027 (2008).

[17] It is commonly thought that this positive charge is provided by oxygen vacancies forming at the surface of LAO [14], rather than by holes (or a cation valence change), such as originally proposed [1,3].

[18] R. Pentcheva and W. E. Pickett, Phys. Rev. B **74**, 035112 (2006).

[19] D. M. Smyth, *The Defect Chemistry of Metal Oxides* (Oxford University Press, New York, 2000).

[20] R. A. De Souza, Phys. Chem. Chem. Phys. **11**, 9939 (2009).

[21] R. A. De Souza, V. Metlenko, D. Park, and T. E. Weirich, Phys. Rev. B **85**, 174109 (2012).

[22] R. A. De Souza, Adv. Funct. Mater. **25**, 6326 (2015).

[23] R. Meyer, R. Waser, J. Helmbold, and G. Borchardt, Phys. Rev. Lett. **90**, 105901 (2003).

[24] K. Gomann, G. Borchardt, A. Gunhold, W. Maus-Friedrichs, and H. Baumann, Phys. Chem. Chem. Phys. **6**, 3639 (2004).

[25] R. Moos and K. H. Haerdtl, J. Am. Ceram. Soc. **80**, 2549 (1997).

[26] R. Waser, J. Am. Ceram. Soc. **74**, 1934 (1991).

[27] R. A. De Souza, F. Gunkel, S. Hoffmann-Eifert, and R. Dittmann, Phys. Rev. B **89**, 241401 (2014).

[28] See Supplemental Material at http://link.aps.org/supplemental/10.1103/PhysRevB.93.245431 for bulk calculations (Sec. I), long-range defect concentration profiles (Sec. II), and *p*-type interface calculations (Sec. III).

[29] Y. Li, S. N. Phattalung, S. Limpijumnong, J. Kim, and J. Yu, Phys. Rev. B **84**, 245307 (2011).

[30] For diluted systems $[c_{def}(x) \ll N_{def}]$, this reduces to the well-known expressions

$$c_{def}(x) = c_{def}^b e^{[-z_{def}e\Phi(x)/k_BT]},$$

i.e., exponential depletion/accumulation of charged defect species.

[31] J. Maier, G. Schwitzgebel, and H.-J. Hagemann, J. Solid State Chem. **58**, 1 (1985).

[32] C. L. Jia, S. B. Mi, M. Faley, U. Poppe, J. Schubert, and K. Urban, Phys. Rev. B **79**, 081405(R) (2009).

[33] C. Cantoni, J. Gazquez, F. M. Granozio, M. P. Oxley, M. Varela, A. R. Lupini, S. J. Pennycook, C. Aruta, U. S. di Uccio, P. Perna, and D. Maccariello, Adv. Mater. **24**, 3952 (2012).

[34] M. P. Warusawithana, C. Richter, J. A. Mundy, P. Roy, J. Ludwig, S. Paetel, T. Heeg, A. A. Pawlicki, L. F. Kourkoutis, M. Zheng, M. Lee, B. Mulcahy, W. Zander, Y. Zhu, J. Schubert, J. N. Eckstein, D. A. Muller, C. S. Hellberg, J. Mannhart, and D. G. Schlom, Nat. Commun. **4**, 2351 (2013).

[35] H. K. Sato, C. Bell, Y. Hikita, and H. Y. Hwang, Appl. Phys. Lett. **102**, 251602 (2013).

[36] F. Gunkel, S. Hoffmann-Eifert, R. Dittmann, S. Mi, C. Jia, P. Meuffels, and R. Waser, Appl. Phys. Lett. **97**, 012103 (2010).

[37] R. C. Neville, B. Hoeneisen, and C. A. Mead, J. Appl. Phys. **43**, 2124 (1972).

[38] At low temperature, where STO has a tetragonal structure, this is not valid anymore and the field dependence of the dielectric constant has to considered [39,40].

[39] M. Minohara, Y. Hikita, C. Bell, H. Inoue, M. Hosoda, H. K. Sato, H. Kumigashira, M. Oshima, E. Ikenaga, and H. Y. Hwang, arXiv:1403.5594.

[40] O. Copie, V. Garcia, C. Bodefeld, C. Carrétéro, M. Bibes, G. Herranz, E. Jacquet, J.-L. Maurice, B. Vinter, S. Fusil, K. Bouzehouane, H. Jaffrès, and A. Barthélémy, Phys. Rev. Lett. **102**, 216804 (2009).

[41] S. Gariglio, A. Fête, and J.-M. Triscone, J. Phys.: Condens. Matter **27**, 283201 (2015).

[42] Growth-induced intermixing of cations into STO will add an additional term to $\rho(x)$. However, cation intermixing is confined to the very interface region. Thus, $\rho(x)$ is only significantly affected, if the density of intermixed cations, e.g., $La_{Sr}^{\bullet}$ or Al_{Ti}' [14], exceed the near surface concentration of defect species considered to be mobile. As shown in the main text, these are as high as several atomic percent. Donor-type $La_{Sr}^{\bullet}$ further increases the required amount of negative charge accumulation in the SCL.

[43] S. M. Sze and K. K. Ng, *Physics of Semiconductor Devices* (Wiley, New York, 2007).

[44] G. Drera, G. Salvinelli, A. Brinkman, M. Huijben, G. Koster, H. Hilgenkamp, G. Rijnders, D. Visentin, and L. Sangaletti, Phys. Rev. B **87**, 075435 (2013).

[45] A. H. H. Ramadan, N. L. Allan, and R. A. De Souza, J. Am. Ceram. Soc. **96**, 2316 (2013).

[46] L. Zhang, X.-F. Zhou, H.-T. Wang, J.-J. Xu, J. Li, E. G. Wang, and S.-H. Wei, Phys. Rev. B **82**, 125412 (2010).

[47] R. Waser, R. Bruchhaus, and S. Menzel, in *Nanoelectronics and Information Technology*, 3rd ed., edited by R. Waser (Wiley-VCH, Berlin, 2012), pp. 683–710.

[48] S. Menzel, M. Salinga, U. Bttger, and M. Wimmer, Adv. Funct. Mater. **25**, 6306 (2015).

[49] G. Berner, S. Glawion, J. Walde, F. Pfaff, H. Hollmark, L.-C. Duda, S. Paetel, C. Richter, J. Mannhart, M. Sing, and R. Claessen, Phys. Rev. B **82**, 241405(R) (2010).

[50] C. Cancellieri, N. Reyren, S. Gariglio, A. D. Caviglia, A. Fête, and J. Triscone, Europhys. Lett. **91**, 17004 (2010).

[51] N. Reyren, S. Thiel, A. D. Caviglia, L. F. Kourkoutis, G. Hammerl, C. Richter, C. W. Schneider, T. Kopp, A.-S. Ruetschi, D. Jaccard, M. Gabay, D. A. Muller, J. M. Triscone, and J. Mannhart, Science **317**, 1196 (2007).

[52] L. Li, C. Richter, J. Mannhart, and R. C. Ashoori, Nat. Phys. **7**, 762 (2011).

[53] Ariando, X. Wang, G. Baskaran, Z. Q. Liu, J. Huijben, J. B. Yi, A. Annadi, A. R. Barman, A. Rusydi, S. Dhar, Y. P. Feng, J. Ding, H. Hilgenkamp, and T. Venkatesan, Nat. Commun. **2**, 188 (2011).

[54] G. Khalsa and A. H. MacDonald, Phys. Rev. B **86**, 125121 (2012).

[55] G. Berner, M. Sing, H. Fujiwara, A. Yasui, Y. Saitoh, A. Yamasaki, Y. Nishitani, A. Sekiyama, N. Pavlenko, T. Kopp, C. Richter, J. Mannhart, S. Suga, and R. Claessen, Phys. Rev. Lett. **110**, 247601 (2013).

[56] C. Xu, C. Bäumer, R. A. Heinen, S. Hoffmann-Eifert, F. Gunkel, and R. Dittmann, Sci. Rep. **6**, 22410 (2016).

[57] M. L. Reinle-Schmitt, C. Cancellieri, A. Cavallaro, G. F. Harrington, S. J. Leake, E. Pomjakushina, J. A. Kilner, and P. R. Willmott, Nanoscale **6**, 2598 (2014).

[58] C. W. Bark, D. A. Felker, Y. Wang, Y. Zhang, H. W. Jang, C. M. Folkman, J. W. Park, S. H. Baek, H. Zhou, D. D. Fong, X. Q. Pan, E. Y. Tsymbal, M. S. Rzchowski, and C. B. Eom, Proc. Natl. Acad. Sci. USA **108**, 4720 (2011).

[59] Z. Huang, K. Han, S. Zeng, M. Motapothula, A. Y. Borisevich, S. Ghosh, W. L, C. Li, W. Zhou, Z. Liu, M. Coey, T. Venkatesan, and Ariando, Nano Lett. **16**, 2307 (2016).

[60] Y. Z. Chen, N. Bovet, F. Trier, D. V. Christensen, F. M. Qu, N. H. Andersen, T. Kasama, W. Zhang, R. Giraud, J. Dufouleur, T. S. Jespersen, J. R. Sun, A. Smith, J. Nygard, L. Lu, B. Buechner, B. G. Shen, S. Linderoth, and N. Pryds, Nat. Commun. **4**, 1371 (2013).

[61] Y. Chen, N. Pryds, J. E. Kleibeuker, G. Koster, J. Sun, E. Stamate, B. Shen, G. Rijnders, and S. Linderoth, Nano Lett. **11**, 3774 (2011).

[62] F. Trier, S. Amoruso, D. V. Christensen, A. Sambri, Y. Z. Chen, X. Wang, E. Stamate, R. Bruzzese, and N. Pryds, Appl. Phys. Lett. **103**, 031607 (2013).

[63] P. Gallagher, M. Lee, T. A. Petach, S. W. Stanwyck, J. R. Williams, K. Watanabe, T. Taniguchi, and D. Goldhaber-Gordon, Nat. Commun. **6**, 6437 (2015).

[64] N. Ueno and S. Kera, Prog. Surf. Sci. **83**, 490 (2008).

[65] M. Li, W. Han, X. Jiang, J. Jeong, M. G. Samant, and S. S. P. Parkin, Nano Lett. **13**, 4675 (2013).